PWM Nonlinear Control With Load Power Estimation for Output Voltage Regulation of a Boost Converter With Constant Power Load

Blanca Areli Martínez-Treviño, Abdelali El Aroudi, *Senior Member, IEEE*, Hugo Valderrama-Blavi, *Member, IEEE*, Angel Cid-Pastor, *Member, IEEE*, Enric Vidal-Idiarte, *Member, IEEE*, and Luis Martinez-Salamero, *Senior Member, IEEE*

***Abstract*—This article presents a nonlinear control based on pulsewidth modulation (PWM) and an estimation mechanism of the output power to regulate the output voltage of a boost converter supplying a constant power load (CPL). The controller uses three parameters K_p, K_E, and K_A lending the regulator an adaptive nature. The behavior of the latter can be expressed in terms of the dynamic description of three errors. Namely, first, current error, i.e., difference between the average value of the inductor current and its equilibrium value, second, output voltage error, i.e., deviation between the output voltage and its desired equilibrium value, and, second, power error, i.e., difference between the output power estimated value and its actual value. The analysis of the dynamic behavior of the three errors results in a parametric region in the plane $K_p - K_E$ in which the system stability is guaranteed. The regulator exhibits fast and precise responses in the presence of disturbances in the input voltage and the load power. Conduction losses provoke steady-state errors in both current and power estimation but do not affect the output voltage tracking.**

***Index Terms*—Boost converter, constant power load (CPL), nonlinear control, power estimation, pulsewidth modulation (PWM).**

I. Introduction

CONSTANT power supply in the output port of a dc–dc switching converter is a common case in power distribution systems for electric and hybrid vehicles [1]–[6], ships [7]–[9], and microgrids of renewable energy installations [10]–[13]. Since the incremental resistance of a constant power load (CPL) is negative, supplying this type of loads by means of a switching converter can often result in unstable behavior [14]–[17]. Unlike the case with resistive load, converters with CPL are unstable in open loop in continuous conduction mode (CCM) [18], so they can only operate in closed-loop in that mode if an appropriate feedback strategy is used.

Some of the control laws solving the previous problem employ virtual damping, which is introduced by inductor current feedback in the inner loop of a linear cascade control. They aim at stabilizing the system first, and then regulating the output voltage by adding an outer loop that establishes the reference to the inner loop [19]–[22]. The outer-loop design is based on a dynamic model of the converter that includes the effect of the current inner loop. Nonetheless, the resulting model can be still unstable in certain cases [23], so the outer loop has to counteract this instability and ensure the output voltage regulation at the same time. In most of the cases, the resulting switching regulator perfectly attenuates the effect of the small-signal disturbances penetrating into the system. A recent example of virtual damping can be found in [24]. In that work, a control law transforms the nonlinear inductor current dynamics in a boost converter into a linear inductor current dynamics in a virtual mesh, in which a resistance introduces damping into the system and a voltage source indirectly provides the output voltage regulation. The control scheme has only one feedback loop and no separated dynamics between inductor current and capacitor voltage are considered. Another approach to tackle the problem has been carried out by means of different alternatives of nonlinear control such as input–output linearization [25], boundary control [26], [27], or sliding-mode control (SMC) [28]–[32].

The common feature of the latter controllers is their theoretical nature, their objective being to prove in each case that the proposed control succeeds in stabilizing an intrinsically unstable system. Other important issues such as mitigation of the effects due to the input voltage or load power variations, minimization of the inrush current or practical realization of the converter are hardly reported in the literature. A SMC based on a switching surface made up of a linear combination of both inductor current and capacitor voltage errors regarding their respective equilibrium values was proposed in [33] with the aim of covering the previous issues and tackling the problem of regulating the converter under large-signal operation. The resulting control provides output voltage regulation in the presence of variations in both input voltage and load power and

Manuscript received March 12, 2020; revised June 1, 2020; accepted July 3, 2020. Date of publication July 8, 2020; date of current version September 22, 2020. This work was supported in part by the Spanish Agencia Estatal de Investigación (AEI) and in part by the Fondo Europeo de Desarrollo Regional (FEDER) under Grants DPI2017-84572-C2-1-R, DPI2016-80491-R(AEI/FEDER, UE), and DPI2015-67292-R. Recommended for publication by Associate Editor C. K. Tse. *(Corresponding author: Blanca Areli Martínez-Treviño.)*

The authors are with the Group of Automatic Control and Industrial Electronics (GAEI), Department of Electrical, Electronic and Automatic Control Engineering, School of Electrical and Computer Engineering, Rovira i Virgili University, 43007 Tarragona, Spain (e-mail: blancaareli.martinez@urv.cat; abdelali.elaroudi@urv.cat; hugo.valderrama@urv.cat; angel.cid@urv.cat; enric.vidal@urv.cat; luis.martinez@urv.cat).

Color versions of one or more of the figures in this article are available online at https://ieeexplore.ieee.org.

Digital Object Identifier 10.1109/TPEL.2020.3008013

yields a very low value of the inrush current at the expense of variable switching frequency and the utilization of four sensors to measure output voltage, input voltage, inductor current and CPL current, respectively.

Regarding uncertainty in the CPL, the work in [34] introduces an adaptive-based controller for the output voltage regulation of a buck–boost converter with unknown power load. Although the proposal is interesting from a theoretical point of view, is unpractical from an engineering perspective. The approach is modified in [35] by means of a change of coordinates and partial linearization that yields a cascade control with an inner loop based on energy-shaping and an outer loop with PI compensation for output voltage regulation. The resulting control is apparently feasible for practical execution but no details about its final digital implementation are reported.

The main goal of this article is to present a new simple nonlinear pulsewidth modulation (PWM) based controller for output voltage regulation of a boost converter supplying a CPL with power uncertainty. With the new controller, the drawbacks observed in [33] are relieved. Thus, the controller ensures a converter operation at constant switching frequency, it only requires measuring both input and output voltages plus the inductor current, and is easily implementable using standard analog devices. The information on the CPL power is obtained by means of an estimation loop, which gives the system an adaptive behavior.

The rest of this article is organized as follows. The proposed control is described in Section II. The state equations that describe the closed-loop behavior of the system are analyzed in Section III. The study of the stability is covered in Section IV while simulation and experimental results are reported in Section V. The effect of conduction losses in the tracking of inductor current, output voltage, and output power is studied in Section VI. Finally, Section VII concludes the article.

II. Proposed Nonlinear Controller

A. Open-Loop Boost Converter Averaged Model

Fig. 1 shows the block diagram of the boost converter with CPL and the proposed PWM-based nonlinear control with output power estimation. The purpose of auxiliary diode $\mathrm{D_a}$ is to minimize the effect of the inrush current in the inductor. Variable u is a binary signal that activates or deactivates MOSFET Q and takes the values 1 and 0 in the ON and OFF states, respectively.

In CCM, the average behavior of the converter can be expressed as follows [36]:

$$\frac{d\overline{i_L}}{dt} = -\frac{(1-d)}{L}\overline{v_C} + \frac{V_g}{L} \tag{1a}$$

$$\frac{d\overline{v_C}}{dt} = \frac{(1-d)}{C}\overline{i_L} - \frac{P}{C\overline{v_C}} \tag{1b}$$

where $\overline{i_L}$ and $\overline{v_C}$ are, respectively, the averaged values of the inductor current i_L and output capacitor voltage v_C in a switching period, and d is the duty cycle of the driving signal u.

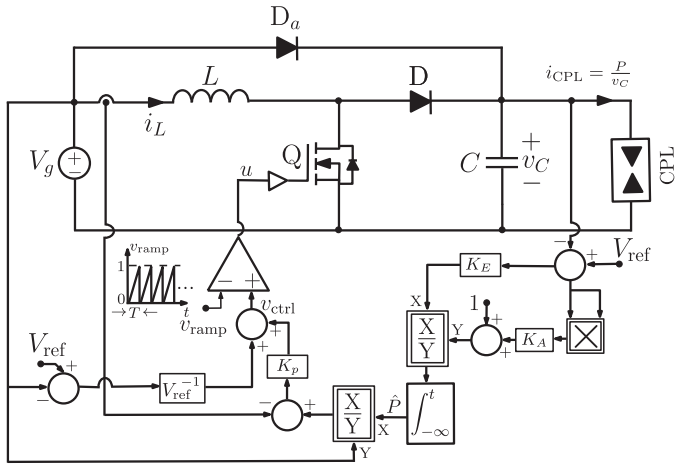

Fig. 1. Block diagram of a PWM-based nonlinear control with output power estimation in a boost converter with CPL.

B. PWM Nonlinear Control Law

This section introduces a nonlinear control for the output voltage regulation of a boost converter feeding a CPL, where the absorbed power is unknown.

The proposed control law can be expressed as

$$d = \frac{V_{\mathrm{ref}} - V_g}{V_{\mathrm{ref}}} + K_p\left(\frac{\hat{P}}{V_g} - \overline{i_L}\right) \tag{2}$$

where V_{ref} is the desired output voltage and $\hat{P}$ represents the estimated load power whose dynamic behavior is given by the following nonlinear differential equation

$$\frac{d\hat{P}}{dt} = \frac{K_E(V_{\mathrm{ref}} - \overline{v_C})}{1 + K_A(V_{\mathrm{ref}} - \overline{v_C})^2}. \tag{3}$$

A detailed explanation of the origin of (2) and (3) has been included in Appendix A.

Note that variable d in Fig. 1 is introduced as a duty cycle in a pulse width modulator and compared with a high-frequency periodic sawtooth signal v_{ramp} whose maximum value is equal to one. Signal v_{ramp} establishes the switching period T and its comparison with the control voltage v_{ctrl} determines the duration of the ON state in each switching cycle and, therefore, the duty cycle d in that cycle.

In addition, it can be observed that the control law has two terms. The first one is $(V_{\mathrm{ref}} - V_g)/V_{\mathrm{ref}}$ that constitutes the duty cycle required in steady-state once the nominal values of input and output voltages are set. The second term acts as corrective element during the transient-state and is proportional to the current error, i.e., the difference between the actual average value of the inductor current and its steady-state value provided that the estimated power is the power delivered in the output port to the CPL.

It is worth mentioning that the time-derivative of the estimated variable is an odd-symmetry function of the output voltage error that eventually will be responsible of the adaptive behavior of the control [37]. In that function, parameter K_A is directly

related to the maximum absolute value of $d\hat{P}/dt$, so selecting K_A, establishes by design $|d\hat{P}/dt|_{\max}$ and, therefore, limits the subsequent integration avoiding saturation. The latter property is demonstrated in Appendix B. This adaptive mechanism has been successfully used in the case of a fourth-order voltage step-up converter with resistive load [38].

III. State Equations for the Closed-Loop Switching Converter

The introduction of (2) and (3) in (1a) and (1b) leads to the closed-loop dynamical model of the system that is given by the following set of differential equations:

$$\frac{d\overline{i_L}}{dt} = -\frac{1}{L}\left(\frac{V_g}{V_{\rm ref}} - K_p\left(\frac{\hat{P}}{V_g} - \overline{i_L}\right)\right)\overline{v_C} + \frac{V_g}{L} \tag{4a}$$

$$\frac{d\overline{v_C}}{dt} = \frac{1}{C}\left(\frac{V_g}{V_{\rm ref}} - K_p\left(\frac{\hat{P}}{V_g} - \overline{i_L}\right)\right)\overline{i_L} - \frac{P}{C\overline{v_C}} \tag{4b}$$

$$\frac{d\hat{P}}{dt} = \frac{K_E(V_{\rm ref} - \overline{v_C})}{1 + K_A(V_{\rm ref} - \overline{v_C})^2}. \tag{4c}$$

Let us define current error e_1, voltage error e_2, and estimated power error e_3 as follows:

$$e_1 = \overline{i_L} - \frac{P}{V_g} \tag{5a}$$

$$e_2 = \overline{v_C} - V_{\rm ref} \tag{5b}$$

$$e_3 = \hat{P} - P. \tag{5c}$$

Therefore, the set of nonlinear equations (4) becomes as given below

$$\frac{de_1}{dt} = -\frac{1}{L}\left(\frac{V_g}{V_{\rm ref}} + K_p\left(\frac{P}{V_g} + e_1\right) - \frac{K_p}{V_g}(P + e_3)\right) \times (V_{\rm ref} + e_2) + \frac{V_g}{L} \tag{6a}$$

$$\frac{de_2}{dt} = \frac{1}{C}\left(\frac{V_g}{V_{\rm ref}} + K_p\left(\frac{P}{V_g} + e_1\right) - \frac{K_p}{V_g}(P + e_3)\right) \times \left(\frac{P}{V_g} + e_1\right) - \frac{P}{C(V_{\rm ref} + e_2)} \tag{6b}$$

$$\frac{de_3}{dt} = -\frac{K_E e_2}{1 + K_A {e_2}^2}. \tag{6c}$$

The coordinates of the equilibrium point of (6) are

$$E_1^* = 0 \quad \Rightarrow \quad \overline{I_L}^* = \frac{P}{V_g} \tag{7a}$$

$$E_2^* = 0 \quad \Rightarrow \quad \overline{V_C}^* = V_{\rm ref} \tag{7b}$$

$$E_3^* = 0 \quad \Rightarrow \quad \hat{P}^* = P. \tag{7c}$$

IV. Stability Analysis

To perform a stability analysis of the equilibrium point given by coordinates (7a)–(7c), let us define y_1, y_2, and y_3 as follows:

$$y_1(t) \triangleq \frac{de_1}{dt} \tag{8a}$$

$$y_2(t) \triangleq \frac{de_2}{dt} \tag{8b}$$

$$y_3(t) \triangleq \frac{de_3}{dt}. \tag{8c}$$

Therefore, the Jacobian matrix corresponding to the linearization of (6a)–(6c) around of the equilibrium point can be expressed as

$$\hat{A} = \begin{bmatrix} \left.\frac{\partial y_1}{\partial e_1}\right|_{X^*} & \left.\frac{\partial y_1}{\partial e_2}\right|_{X^*} & \left.\frac{\partial y_1}{\partial e_3}\right|_{X^*} \\ \left.\frac{\partial y_2}{\partial e_1}\right|_{X^*} & \left.\frac{\partial y_2}{\partial e_2}\right|_{X^*} & \left.\frac{\partial y_2}{\partial e_3}\right|_{X^*} \\ \left.\frac{\partial y_3}{\partial e_1}\right|_{X^*} & \left.\frac{\partial y_3}{\partial e_2}\right|_{X^*} & \left.\frac{\partial y_3}{\partial e_3}\right|_{X^*} \end{bmatrix}$$

$$= \begin{bmatrix} -\frac{K_p V_{\rm ref}}{L} & -\frac{V_g}{LV_{\rm ref}} & \frac{K_p V_{\rm ref}}{LV_g} \\ \frac{V_g}{CV_{\rm ref}} + \frac{K_p P}{CV_g} & \frac{P}{CV_{\rm ref}^2} & -\frac{K_p P}{CV_g^2} \\ 0 & -K_E & 0 \end{bmatrix}. \tag{9}$$

The characteristic equation corresponding to the previous matrix is given by

$$s^3 + \left(\frac{K_p V_{\rm ref}}{L} - \frac{P}{CV_{\rm ref}^2}\right)s^2 + \left(\frac{V_g^2}{LCV_{\rm ref}^2} - \frac{K_E K_p P}{CV_g^2}\right)s + \frac{K_E K_p}{LC} = 0. \tag{10}$$

By simple inspection of (10), the following necessary conditions for stability are derived

$$K_p > \frac{L}{C}\frac{P}{V_{\rm ref}^3} \tag{11a}$$

$$K_p K_E < \frac{V_g^4}{V_{\rm ref}^2}\frac{1}{LP}. \tag{11b}$$

Furthermore, the application of Routh's criterion provides the additional condition

$$K_E < f(K_p) \tag{12}$$

where $f(K_p)$ is defined as follows:

$$f(K_p) \triangleq \frac{\frac{V_g^2}{L^2 C V_{\rm ref}}K_p - \frac{PV_g^2}{LC^2V_{\rm ref}^4}}{K_p\left(\frac{PV_{\rm ref}}{LCV_g^2}K_p + \frac{1}{LC} - \frac{P^2}{C^2 {V_g}^2 V_{\rm ref}^2}\right)}. \tag{13}$$

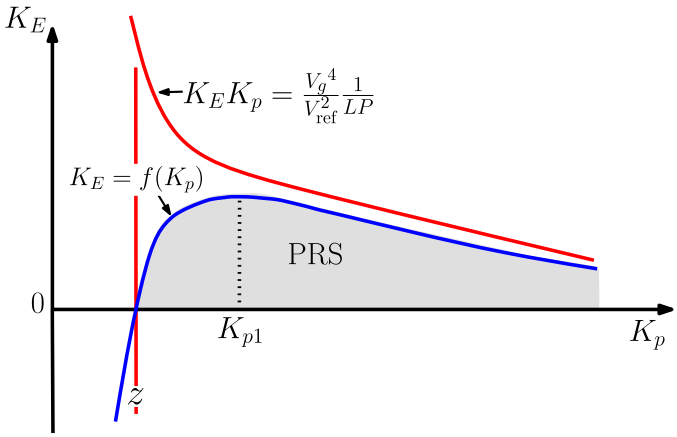

Fig. 2. Parametric region for stability in the plane $K_p - K_E$.

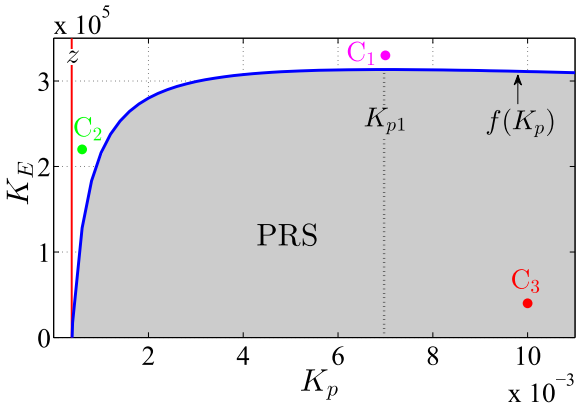

Fig. 3. Three different pairs of parameters $K_p - K_E$.

The parametric constraints given by stability conditions (11a), (11b), and (12) define in Fig. 2, the region colored in grey in the plane $K_p - K_E$ in which the stability is guaranteed. In the parametric region for stability (PRS), $f(K_p)$ is zero for $K_p = z = PL/CV_{\text{ref}}^3$, and has a maximum for $K_p = K_{p1} = (PL/CV_{\text{ref}}) - (V_g\sqrt{L/C}/V_{\text{ref}}^2)$. It can be easily demonstrated that $f(K_p)$ is always under the hyperbola defined by (11b). On the other hand, note that z is equal to the lower boundary value of constraint (11a). Consequently, the system stability will be guaranteed for $K_E < f(K_p)$ and $K_p > z$.

To illustrate the stability predictions derived from Fig. 2, three different cases C_1, C_2, and C_3 are considered in a zoom of the PRS of Fig. 2 depicted in Fig. 3. They correspond to the controller parameters $K_p = 0.007\ \Omega$, $K_E = 340 \times 10^3$ (C_1), $K_p = 6 \times 10^{-4}\ \Omega$, $K_E = 220 \times 10^3\ \Omega$, ($C_2$), and $K_p = 0.01\ \Omega$, $K_E = 40 \times 10^3$ (C_3). The corresponding time domain simulations using the switched model implemented in PSIM software are shown in Fig. 4. As expected, designs C_1 and C_2 result in unstable behavior while C_3 yields stable dynamics. The previous numerical simulations demonstrate the accuracy of the previous theoretical predictions about the stability of the closed-loop system.

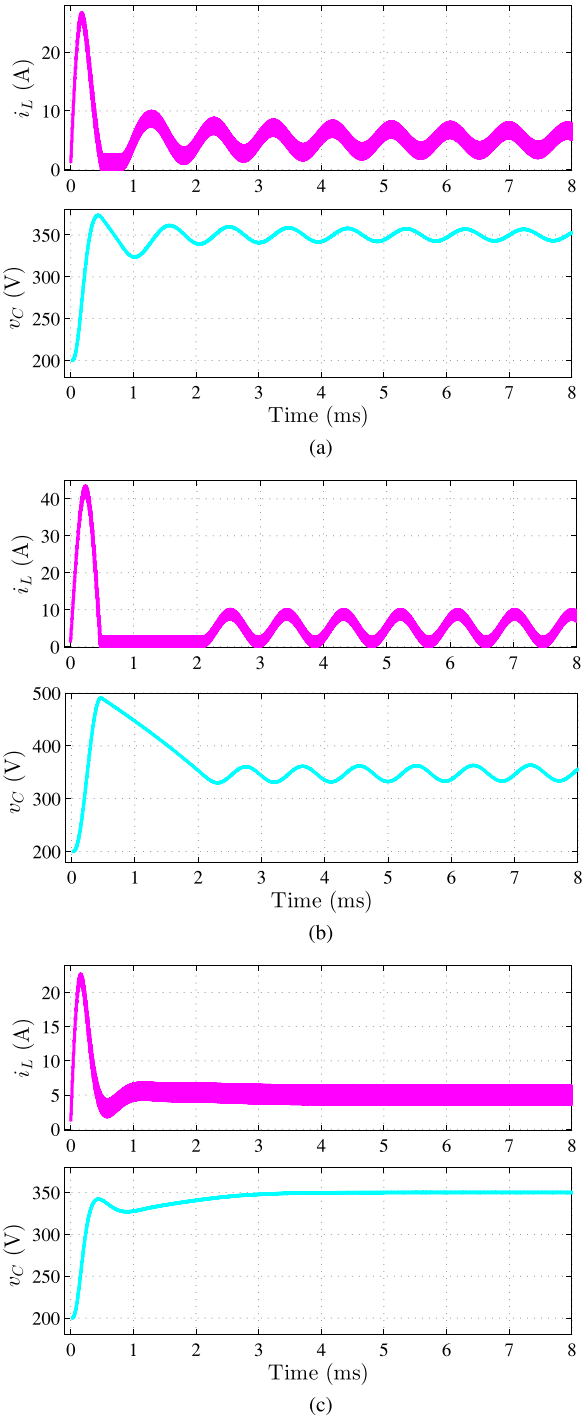

Fig. 4. PSIM simulations of the three different cases of design shown in Fig. 3: (a) case C_1, (b) case C_2, and (c) case C_3.

V. Numerical Simulation and Experimental Results

A. Experimental Prototype

Fig. 5 shows the schematic circuit diagram of an experimental prototype that has been implemented with the following values of parameters: inductance of the inductor $L = 326\ \mu$H, capacitance of the output capacitor $C = 20\ \mu$F, desired reference

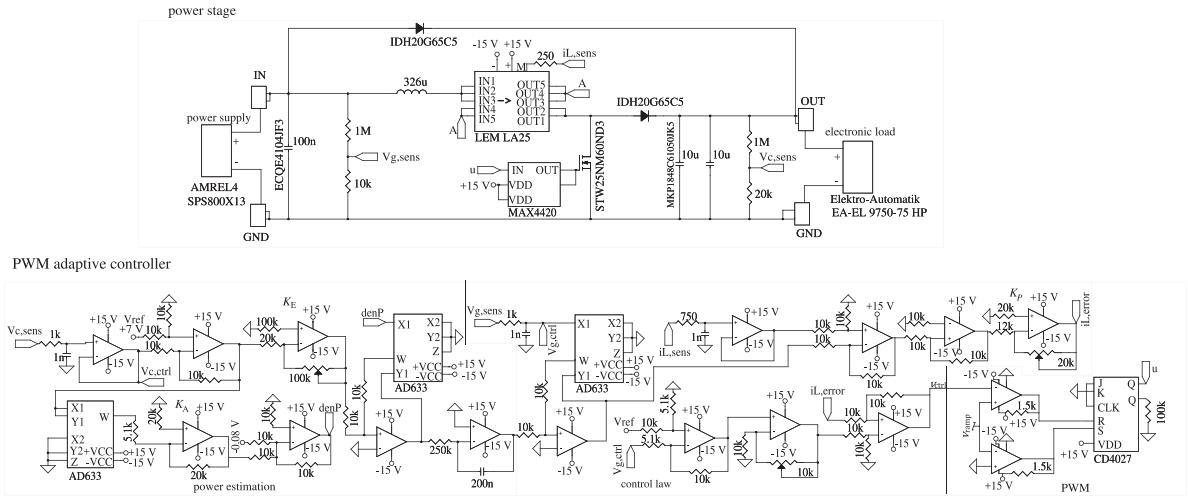

Fig. 5. Circuit scheme of the experimental prototype.

voltage $V_{\rm ref} = 350$ V, nominal values of the CPL power, and the input voltage $P = 1$ kW and $V_g = 200$ V.

Note that stability conditions (11a), (11b), and (12) require the real value of P, which is actually unknown. However, for the selection of K_p and K_E satisfying these conditions, a nominal value of $P = 1$ kW has been used. This value has been employed to design a prototype, which supplies a CPL with an unknown power in the range of 0.5–1 kW. Hence, the controller parameters are $K_p = 0.01\ \Omega$ and $K_E = 40 \times 10^3$ and the switching frequency used is 100 kHz. The complementary action of diode D (IDH20G655G5) and MOSFET Q (IRFP27N60KPBF), which is activated by driver MAX4420, has implemented the switch of the boost converter. The auxiliary diode for startup is the IDH20G655C5. The control voltage $v_{\rm ctrl}$ introduced to the PWM is a small modification of expression (2) because it uses the instantaneous values of the state variables instead of the averaged ones, so no low-pass filtering has been needed. The inductor current has been measured by means of sensor LA25NP with transformer ratio $1/2$ while input and output voltages have been measured by voltage dividers with ratios of $1/50$ and $1/100$, respectively. The operational amplifiers in the control loop are of LF347 type while the analog division is performed by AD633. The sawtooth signal with frequency 100 kHz and amplitude 10 V is provided by function generator Tektronix AFG 202.

The comparator used to generate the PWM signal is LM319, in which the sawtooth signal is internally compared with 10 times signal $v_{\rm ctrl}$, provided by the control loop, in order to adapt the output level of the analog divider to the output level of the function generator. The electronic load EL 9750-75 HP has been used to emulate the CPL. Fig. 6 illustrates the different blocks of the experimental setup.

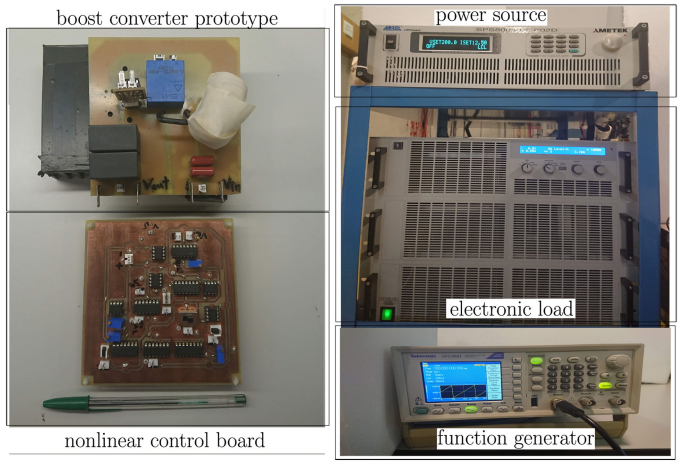

Fig. 6. Blocks of the experimental setup.

B. Simulations and Measurements

Fig. 7 illustrates PSIM simulations and experimental results obtained for the boost switching regulator with the proposed nonlinear control. The figure illustrates the response of the system to input voltage variations. It can be observed that V_g changes from 200 to 250 V with a slope of 6.25 V/ms, and returns from 250 to 200 V with a slope of 13.88 V/ms, such slopes being imposed by the power source AMREL SPS800x13-K02D. The voltage overshoot in the capacitor is of 0.35 % (1.2 V) when the input voltage increases, and the resulting settling time can be neglected. The voltage undershoot, in turn, is of 0.71% (2.5 V) and the settling time is negligible. The inductor current, in turn, changes to its new reference value (4 A) when the input voltage is 250 V while the capacitor voltage recovers the desired value of 350 V after a fast transient-state. A remarkable agreement can be appreciated between the PSIM simulation and the experimental results in the laboratory prototype.

Similarly, the response of the system to step-type changes of the CPL power is shown in Fig. 8, where both simulation and experimental results are depicted. The power of the CPL changes from 1 to 0.5 kW, then remains with this value during 16 ms and returns to its initial value of 1 kW. The voltage overshoot in the capacitor when the power decreases is of 4.57% (17 V), and the associated settling time is of 2 ms. On the other hand, the voltage

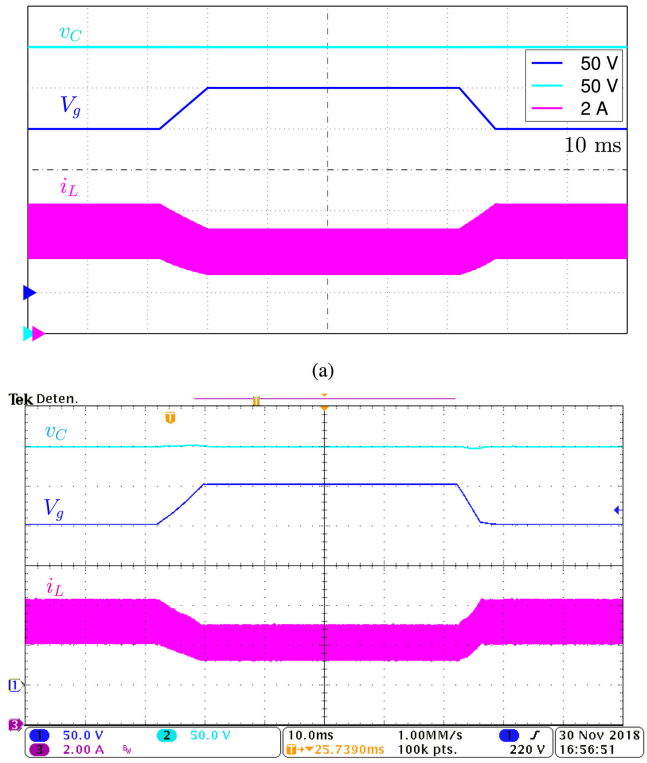

Fig. 7. PSIM simulations (a) and experimental results (b) of the system response in the presence of input voltage variations from 200 to 250 V first, and then from 250 to 200 V.

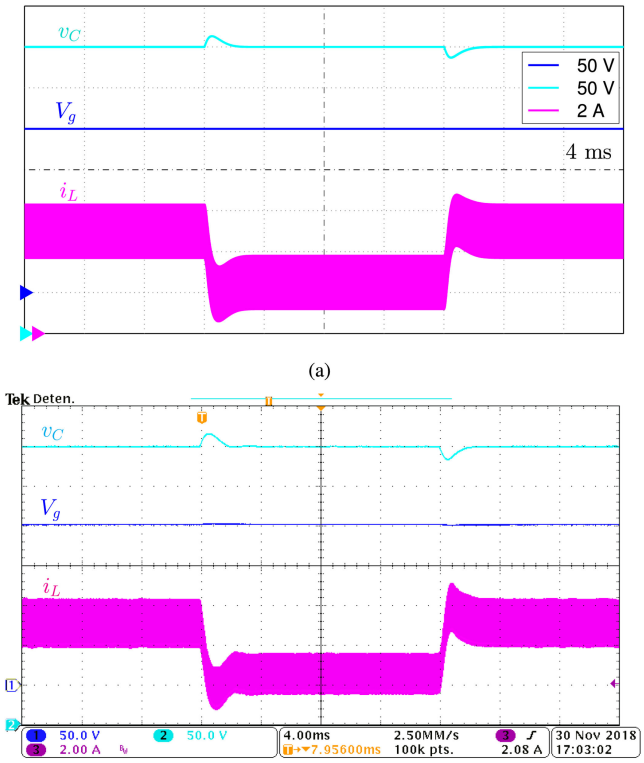

Fig. 8. PSIM simulation (a) and experimental results (b) of the system response for power variations in the CPL from 1 to 0.5 kW first, and then from 0.5 to 1 kW.

undershoot when the power increases is of 4.51% (15.8 V) and the settling time is practically the same than in the previous case. It has to be pointed out the absence of steady-state error in the output voltage.

Moreover, constant switching frequency is observed in both simulated and measured steady-state waveforms in Figs. 9 and 10, where the behavior of the inductor current is illustrated in two different equilibrium points corresponding to input voltages $V_g = 200$ V and $V_g = 250$ V, respectively. Note that the respective averaged values of the inductor current are 5 and 4 A while the switching frequency is 100 kHz in both cases.

Finally, we have performed a comparison on equal basis between the proposed controller and the SMC of a boost converter with CPL reported in [33]. We have selected that work because it exhibited a high degree of output voltage regulation in response to external disturbances, and its theoretical predictions were verified by experiments. The response of the boost converter with CPL under SMC to output power changes is shown in Fig. 11.

By comparing the results in Figs. 8 and 11, we conclude that both strategies show a perfect rejection to load disturbances by recovering the desired output voltage after a short transient-state. The sliding-mode approach has a negligible settling time with no overshoots or undershoots in the output voltage while the PWM nonlinear control has an overshoot around 4.57%. This small overshoot is produced in the lapse during which the estimated power $\hat{P}$ searches the new value of the actual power P. The

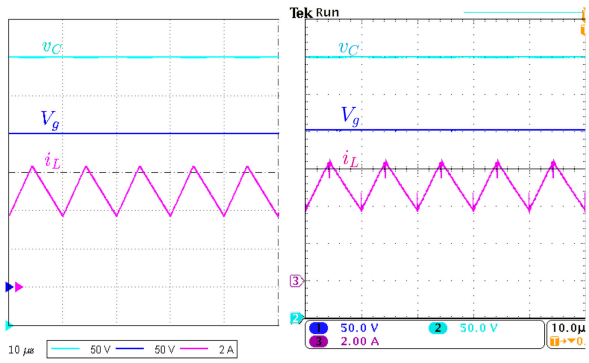

Fig. 9. PSIM simulation (a) and experimental results (b) of the steady-state inductor behavior for $V_g = 200$ V.

fast response of the SMC is intrinsic of that approach because switching between the converter topologies is produced by the internal state of the converter and not by an external signal as in the PWM case.

The practical implementation of the SMC has been carried out with a hysteresis modulator, which eventually results in variable switching frequency. In addition, the implementation of SMC requires the value of the load power. Note that the switching function is given by $S(x) = K_C(v_C - V_{\text{ref}}) + K_L(i_L - P/V_g)$, which includes the term P/V_g that requires the calculation of P

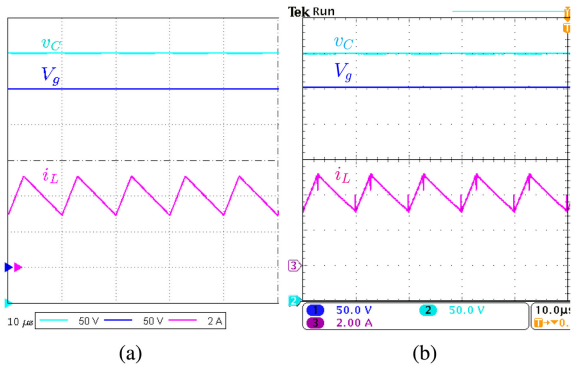

Fig. 10. PSIM simulation (a) and experimental results (b) of the steady-state inductor behavior for $V_g = 250$ V.

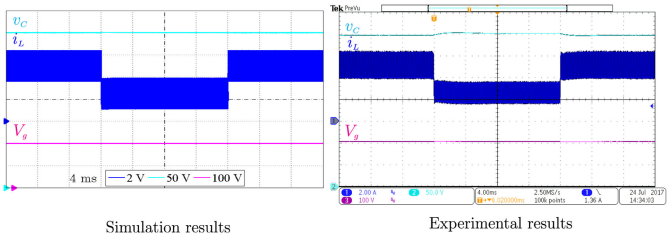

Fig. 11. Response to power load changes of step type from 1 to 0.5 kW and restored back to 1 kW using the SMC reported in [33].

by multiplying the measured values of output voltage and output current. On the contrary, the PWM nonlinear control does not need that current sensor and the associated circuitry to measure the CPL power, and works with constant switching frequency.

VI. Effect of the Losses on the Equilibrium Point

The set of equations (1) describes an ideal behavior of the converter, so no losses have been taken into account. Based on this model, the control law leads to zero steady-state error of the output voltage ($E_2^* = 0$) with respect to the desired value V_{ref} as illustrated in Figs. 7 and 8 in spite of the inevitable converter conduction losses in the implemented prototype. This feature cannot be extended to the other two errors E_1^* and E_3^* corresponding to the inductor current and the estimated power, respectively, which are sensitive to the conduction losses in the circuit. For instance, the simulation of the ideal converter behavior with control law (2) and power estimation (3) shows a perfect tracking of the output power as shown in Fig. 12. It can be observed that variable $\hat{P}$ reaches fast the new value of the CPL power when P changes from 1 to 0.5 kW and from 0.5 to 1 kW.

However, if conduction losses are considered in the converter model, a steady-state error of the estimated power $\hat{P}$ with respect to the actual power P will result. This is shown in Fig. 13(a) and (b), which illustrate simulation and experimental results, respectively. Note again the perfect agreement between both types of results.

The absence of error in the output voltage tracking and the existence of error in the power estimation, and hence, in the

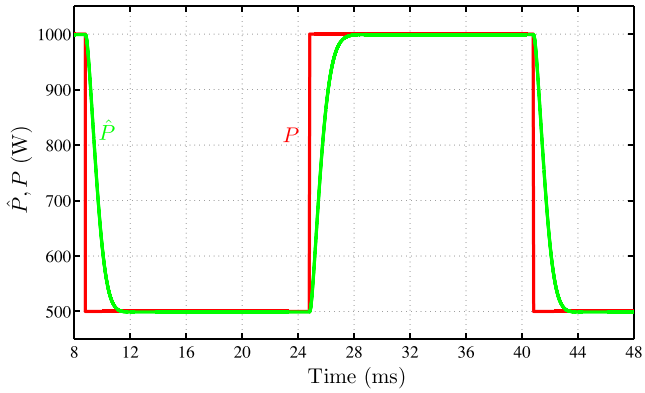

Fig. 12. PSIM simulation of the power estimation behavior.

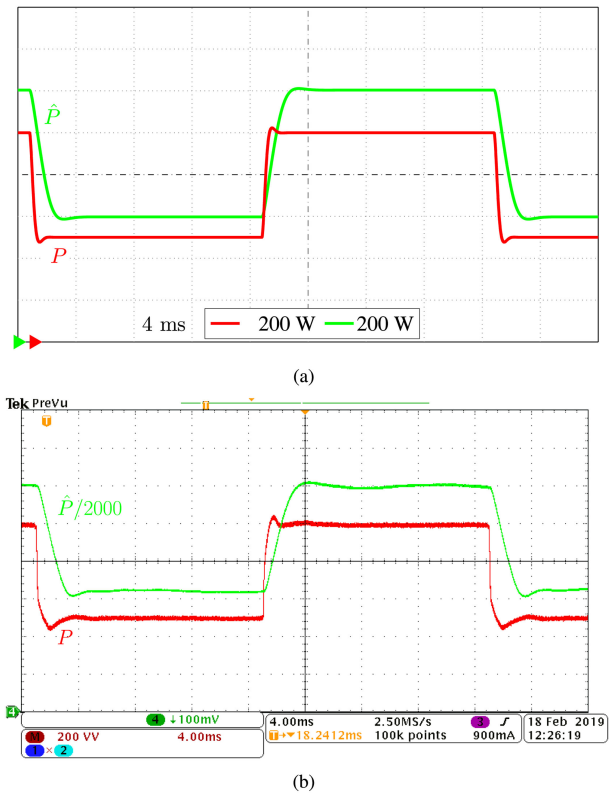

Fig. 13. Effect of the resistive losses on the output power estimation. (a) Simulation results. (b) Experimental results.

inductor current tracking can be explained by modeling, the cumulative effect of conduction losses in inductor, diode, and transistor by means of a resistor R_l in series with inductor L. Taking into account these losses, (6a) becomes as follows:

$$\frac{de_1}{dt} = -\frac{1}{L}\left(\frac{V_g}{V_{\text{ref}}} + K_p\left(\frac{P}{V_g} + e_1\right) - \frac{K_p}{V_g}(P + e_3)\right) \times (V_{\text{ref}} + e_2) - \left(\frac{P}{V_g} + e_1\right)\frac{R_l}{L} + \frac{V_g}{L} \tag{14}$$

while (6b) and (6c) still apply.

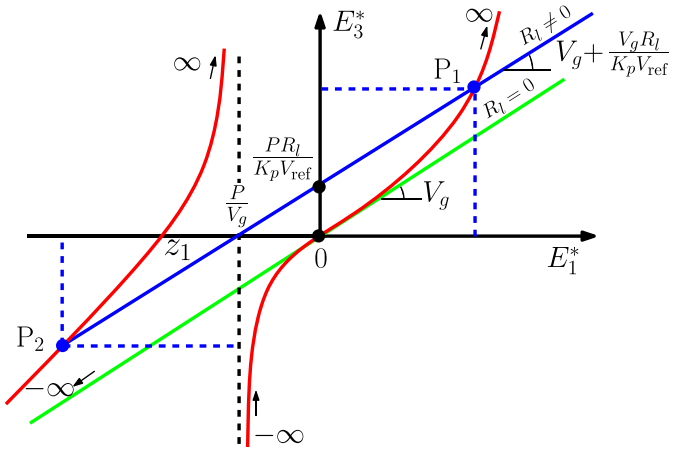

Fig. 14. Graphical representation of (15b) (blue) and (15c) (red).

The analysis of the set of differential equations (6b), (6c), and (14) leads to the following constraints for the coordinates of the equilibrium point

$$E_2^* = 0 \tag{15a}$$

$$E_3^* = \left(V_g + \frac{R_l V_g}{K_p V_{\rm ref}}\right) E_1^* + \frac{PR_l}{K_p V_{\rm ref}} \tag{15b}$$

$$E_3^* = \frac{E_1^* \left(K_p E_1^* + \dfrac{K_p P}{V_g} + \dfrac{V_g}{V_{\rm ref}}\right)}{\dfrac{K_p E_1^*}{V_g} + \dfrac{K_p P}{V_g^2}}. \tag{15c}$$

Expressions (15b) and (15c) can be represented as depicted in Fig. 14. The intersection of curves representing (15b) and (15c) provides two possible values of both E_1^* and E_3^* corresponding to points P_1 and P_2, respectively. In the absence of losses $R_l = 0$, (15b) becomes the green straight line that intersect the red curve only at the origin and at minus infinite, the latter point having no physical meaning. Therefore, for a value of R_l different from zero, there is always a steady-value of E_1^* and E_3^* different from zero. In a clear-cut contrast E_2^* is always zero irrespective of the value of R_l.

It can be demonstrated that modifying the control law (2) by including the effect of losses as follows:

$$d = \frac{2\,V_{\rm ref} - V_g - \hat{\Delta}}{2\,V_{\rm ref}} + K_p \left(\frac{2\hat{P}}{V_g + \hat{\Delta}} - \overline{i_L}\right) \tag{16}$$

where

$$\hat{\Delta} = \sqrt{V_g^2 - 4\hat{P}R_l} \tag{17}$$

yields $E_1^* = E_2^* = E_3^* = 0$ as in the ideal case.

VII. Conclusion

This article has presented a nonlinear control for a dc–dc switching boost converter operating in CCM supplying an unknown constant power load. The proposed strategy uses only three sensors and a pulse width modulator that guarantees a constant switching frequency. The control signal of the PWM has two terms. The first one is the required steady-state duty cycle for given values of input and output voltages. The second one is a compensating element based on the inductor current error with respect to its steady-state value. Given that the latter is unknown because the power of the CPL is unknown, the controller includes a loop processing an odd-symmetry function of the output voltage error to estimate the unknown power. Thus, the controller uses three parameters K_p, K_E, and K_A and combines output power estimation and output voltage regulation with no separated dynamics in a clear-cut contrast with conventional cascade controllers. The closed-loop system behavior has been studied in terms of the joint dynamics of three errors, i.e., output voltage error, inductor current error, and estimated power error. Linearizing the error dynamics has led to a region of stability in the plane defined by the two parameters of the controller K_p and K_E. The third parameter K_A establishes by design $|d\hat{P}/dt|_{\max}$ and, therefore, limits the subsequent integration avoiding saturation.

A subsequent analysis of the conduction losses effect on the controller performance has shown that the tracking of the output voltage is insensitive to that type of losses, so no output voltage error has resulted in steady-state using the control based on a converter model without losses. The analysis has also demonstrated that steady-state errors will exist in both inductor current and estimated power in presence of conduction losses. Reformulating the control law with the inclusion of a term modeling the losses has led to zero steady-state error in both inductor current and power estimation. Nonetheless, the reformulation has only a theoretical interest since its implementation would require measuring offline the parasitic resistance of each element in the inductor current path in both ON and OFF states to group all the losses together in a single resistor R_l. For that reason, the control derived from the ideal model of the converter is preferred since offers a robust behavior of the voltage regulation in presence of uncertainty not only in the output power but also in the parasitic resistances.

The experimental results have verified both theoretical and simulation predictions for large-signal variations of input voltage and CPL power. A comparison on equal basis with a sliding-mode strategy has shown that the control here proposed results in a similar dynamic response adding constant switching frequency and not requiring output current sensing to calculate the power of the CPL.

Appendix A
Analysis of the Proposed Control Law

Assuming in (2) that the duty cycle is limited to the first term, results in

$$d = \frac{V_{\rm ref} - V_g}{V_{\rm ref}}. \tag{A.1}$$

In steady state, the output voltage will be given by

$$\overline{V_C} = V_{\rm ref} = \frac{V_g}{1 - D}. \tag{A.2}$$

This is the expected behavior of the boost converter in open loop. Nonetheless, we need to add a term to counteract the disturbances introduced through input and output ports, i.e., input voltage variations and power demand changes.

The new term should keep constant the output voltage and redirect the energy introduced by the disturbances to the inductor current. While the equilibrium coordinate of the output voltage must be preserved, that of the inductor current must change to absorb the increment of energy penetrating into the system. Thus, the coordinate of the inductor current equilibrium point becomes a function of time.

After a transient-state created by an external disturbance, the regulated system only changes the inductor current equilibrium point while keeping constant the coordinate of the capacitor voltage. A traditional procedure to implement the corresponding control is to include a linear function of the output voltage error in the expression of the coordinate of the inductor current equilibrium point, which is used to process the inductor current error [39].

Therefore, (A.2) could be modified as follows:

$$d = \frac{V_{\rm ref} - V_g}{V_{\rm ref}} + K_p(i_E(t) - \overline{i_L}) \tag{A.3}$$

where $(i_E(t) - \overline{i_L})$ is the inductor current error, and $i_E(t)$ is the time-varying coordinate of the inductor current equilibrium coordinate given by

$$i_E(t) = I_E + \hat{i}_E(t). \tag{A.4}$$

In the last expression, I_E is the inductor current coordinate in the equilibrium point corresponding to nominal values of input voltage and output power, i.e., $I_E = P/V_g$. In addition, $\hat{i}_E(t)$ is the time-varying term for indirect output voltage regulation.

Hence, a possible expression of (A.3) could be given by

$$d = \frac{V_{\rm ref} - V_g}{V_{\rm ref}} + K_p\left(\frac{P}{V_g} + \hat{i}_E(t) - \overline{i_L}\right) \tag{A.5}$$

where $\hat{i}_E(t)$ could be defined as follows:

$$\hat{i}_E(t) = K_1(V_{\rm ref} - \overline{v_C}) + K_2\int_{-\infty}^{t}(V_{\rm ref} - \overline{v_C}(\lambda))d\lambda. \tag{A.6}$$

Hence, introducing (A.6) in (A.5) results in

$$d = \frac{V_{\rm ref} - V_g}{V_{\rm ref}} + K_p\left(\frac{P}{V_g} + K_1(V_{\rm ref} - \overline{v_C}) + K_2\int_{-\infty}^{t}(V_{\rm ref} - \overline{v_C}(\lambda))d\lambda - \overline{i_L}\right). \tag{A.7}$$

However, expression (A.7) has the following drawbacks.

1) The term P/V_g is unknown in the problem studied in this article because P is unknown.
2) The term $K_2\int_{-\infty}^{t}(V_{\rm ref} - \overline{v_C}(\lambda))d\lambda$ can be saturated since it is the integral of a linear expression of the voltage error. The higher the error is the higher the integral results and the risk of saturation increases in a real implementation.

Therefore, the term P/V_g has to be estimated by means of $\hat{P}/V_g$ while the indirect regulation of the output voltage given by (A.6) will be performed through $\hat{P}$, which, in turn, will be given by

$$\hat{P} = \int_{-\infty}^{t}\frac{K_E(V_{\rm ref} - \overline{v_C})}{1 + K_A(V_{\rm ref} - \overline{v_C})^2}. \tag{A.8}$$

Expression (A.8) is the integral of a bounded function whose maximum value can be established by an appropriate choice of parameter $K_{\rm A}$ as shown in Appendix B.

Therefore, the final control law becomes

$$d = \frac{V_{\rm ref} - V_g}{V_{\rm ref}} + K_p\left(\frac{\int_{-\infty}^{t}\frac{K_E(V_{\rm ref} - \overline{v_C})}{1 + K_A(V_{\rm ref} - \overline{v_C})^2}}{V_g} - \overline{i_L}\right) \tag{A.9}$$

which corresponds to (2) and (3).

APPENDIX B
EXAMINATION OF PARAMETER K_A

The power estimator dynamics in (3) can be rewritten as follows:

$$y = \frac{K_E x}{1 + K_A x^2} \tag{B.1}$$

being $y = d\hat{P}/dt$ and $x = V_{\rm ref} - \overline{v_C}$.

It can be noted that (B.1) is an odd-symmetry function of the output voltage error, which has a minimum for $x_{\min} = -1/\sqrt{K_{\rm A}}$ and a maximum for $x_{\max} = 1/\sqrt{K_{\rm A}}$. Besides, the absolute value of the function is the same in both extrema and can be expressed as follows:

$$|y|_{\max} = \frac{K_E}{2\sqrt{K_A}}. \tag{B.2}$$

Or equivalently, the maximum absolute value of the time derivative of the estimated variable is given by

$$\left|\frac{d\hat{P}}{dt}\right|_{\max} = \frac{K_E}{2\sqrt{K_A}}. \tag{B.3}$$

Therefore, the gain K_A is essential to limit the maximum absolute value of the estimated variable derivative. Then, the maximum value of the function to be integrated is limited by design, which avoids saturation of the integrator, in a clear-cut contrast by using a linear function of the voltage error as the one shown in (A.6). In addition, even for large voltage error values, the function to be integrated approaches to zero and the integral will not be saturated, as is shown below

$$\lim_{x\to\infty}\frac{K_E x}{1 + K_A x^2} = 0. \tag{B.4}$$

On the other hand, the gain K_A is not part of the stability analysis around of the equilibrium point because the linearization of (B.1) around that point is equivalent to substitute this expression by the tangent to the curve at the origin, which leads to

$$y_{\rm lin} = \left.\frac{dy}{dx}\right|_{x=0} x = K_E x. \tag{B.5}$$

Fig. 15 represents function (B.1) in the plane x–y for two different values of K_A. The maximum and minimum of function

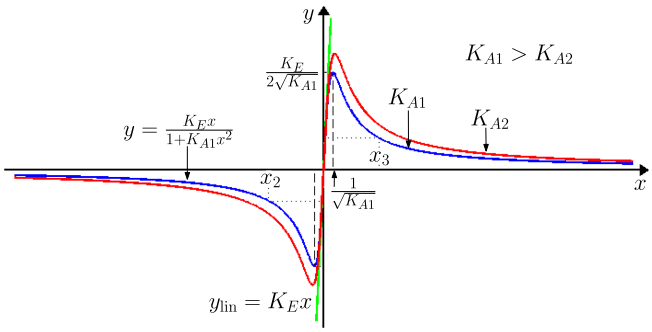

Fig. 15 Graphical representation of the power estimator dynamics.

y and its linear approximation y_{lin} close to the origin can also be observed. Furthermore, function y has three inflection points at $x_1 = 0$, $x_2 = -\sqrt{1/K_A}$, and $x_3 = \sqrt{1/K_A}$, respectively.

REFERENCES

[1] C. Rivetta, G. A. Williamson, and A. Emadi, "Constant power loads and negative impedance instability in sea and undersea vehicles: statement of the problem and comprehensive large-signal solution," *IEEE Elect. Ship Technol. Symp.*, Jul. 2005, pp. 313–320.

[2] A. Emadi, A. Khaligh, C. H. Rivetta, and G. A. Williamson, "Constant power loads and negative impedance instability in automotive systems: Definition, modeling, stability, and control of power electronic converters and motor drives," *IEEE Trans. Veh. Technol.*, vol. 55, no. 4, pp. 1112–1125, Jul. 2006.

[3] C. H. Rivetta, A. Emadi, G. A. Williamson, R. Jayabalan, and B. Fahimi, "Analysis and control of a buck dc-dc converter operating with constant power load in sea and undersea vehicles," *IEEE Trans. Ind. Appl.*, vol. 42, no. 2, pp. 559–572, Mar. 2006.

[4] A. Khaligh, "Realization of parasitics in stability of dc–dc converters loaded by constant power loads in advanced multiconverter automotive systems," *IEEE Trans. Ind. Electron.*, vol. 55, no. 6, pp. 2295–2305, Jun. 2008.

[5] A. M. Rahimi and A. Emadi, "An analytical investigation of DC/DC power electronic converters with constant power loads in vehicular power systems," *IEEE Trans. Veh. Technol.*, vol. 58, no. 6, pp. 2689–2702, Jul. 2009.

[6] S. C. Smithson and S. S. Williamson, "Constant power loads in more electric vehicles—An overview," in *Proc. 38th Annu. Conf. IEEE Ind. Electron. Soc.*, Oct. 2012, pp. 2914–2922.

[7] I. Kondratiev and R. Dougal, "Synergetic control strategies for shipboard DC power distribution systems," in *Proc. Amer. Control Conf.*, Jul. 2007, pp. 4744–4749.

[8] Y. Zhao, W. Qiao, and D. Ha, "A sliding-mode duty-ratio controller for DC/DC buck converters with constant power loads," *IEEE Trans. Ind. Appl.*, vol. 50, no. 2, pp. 1448–1458, Mar. 2014.

[9] L. C. A. J. Mills and R. W. Ashton, "Multi-rate LQR control of a multi-machine MVDC shipboard electric distribution system with constant power loads," in *Proc. IEEE 60th Int. Midwest Symp. Circuits Syst.*, Aug. 2017, pp. 1380–1385.

[10] A. Kwasinski and C. N. Onwuchekwa, "Dynamic behavior and stabilization of dc microgrids with instantaneous constant-power loads," *IEEE Trans. Power Electron.*, vol. 26, no. 3, pp. 822–834, Mar. 2011.

[11] X. Lu, K. Sun, J. M. Guerrero, J. C. Vasquez, L. Huang, and J. Wang, "Stability enhancement based on virtual impedance for dc microgrids with constant power loads," *IEEE Trans. Smart Grid*, vol. 6, no. 6, pp. 2770–2783, Nov. 2015.

[12] M. K. AL-Nussairi, R. Bayindir, S. Padmanaban, L. Mihet-Popa, and P. Siano, "Constant power loads (CPL) with microgrids: Problem definition, stability analysis and compensation techniques," *Energies*, vol. 10, no. 10, p. 1656, Oct. 2017.

[13] X. Chang, Y. Li, X. Li, and X. Chen, "An active damping method based on a supercapacitor energy storage system to overcome the destabilizing effect of instantaneous constant power loads in DC microgrids," *IEEE Trans. Energy Convers.*, vol. 32, no. 1, pp. 36–47, Mar. 2017.

[14] M. Belkhayat, R. Cooley, and A. Witulski, "Large signal stability criteria for distributed systems with constant power loads," in *Proc. 26th Annu. IEEE Power Electron. Specialists Conf.*, Jun. 1995, vol. 2, pp. 1333–1338.

[15] A. Emadi and A. Ehsani, "Dynamics and control of multi-converter dc power electronic systems," in *Proc. IEEE 32nd Annu. Power Electron. Specialists Conf.*, Aug. 2001, vol. 1, pp. 248–253.

[16] S. Singh, A. R. Gautam, and D. Fulwani, "Constant power loads and their effects in DC distributed power systems: A review," *Renew. Sustain. Energy Rev.*, vol. 72, pp. 407–421, May 2017.

[17] E. Hossain, R. Perez, A. Nasiri, and S. Padmanaban, "A comprehensive review on constant power loads compensation techniques," *IEEE Access*, vol. 6, pp. 33 285–33 305, 2018.

[18] A. M. Rahimi and A. Emadi, "Discontinuous-conduction mode dc/dc converters feeding constant-power loads," *IEEE Trans. Industrials Electron.*, vol. 57, no. 4, pp. 1318–1329, Apr. 2010.

[19] A. M. Rahimi and A. Emadi, "Active damping in DC/DC power electronic converters: A novel method to overcome the problems of constant power loads," *IEEE Trans. Industrials Electron.*, vol. 56, no. 5, pp. 1428–1439, May 2009.

[20] Y. Li, K. R. Vannorsdel, A. J. Zirger, M. Norris, and D. Maksimovic, "Current mode control for boost converters with constant power loads," *IEEE Trans. Circuit Syst. I: Reg.*, vol. 59, no. 1, pp. 198–206, Jan. 2012.

[21] A. El Aroudi, B. A. Martinez-Treviño, E. Vidal-Idiarte, and L. Martinez-Salamero, "Mitigating the problem of inrush current in a digital sliding mode controlled boost converter taking into account load and inductor nonlinearities and propagation delay in the feedback loop," in *Proc. IEEE Int. Symp. Circuits Syst.*, Sapporo, Japan, May 2019, pp. 1–5.

[22] A. El Aroudi, B. A. Martínez-Treviño, E. Vidal-Idiarte, and A. Cid-Pastor, "Fixed switching frequency digital sliding-mode control of dc-dc power supplies loaded by constant power loads with inrush current limitation capability," *Energies*, vol. 12, no. 6, p. 1055, Mar. 2019.

[23] B. Choi, B. H. Cho, and S. S. Hong, "Dynamics and control of DC-to-DC converters driving other converters downstream," *IEEE Trans. Circuits Syst. I: Fundam. Theory Appl.*, vol. 46, no. 10, pp. 1240–1248, Oct. 1999.

[24] B. A. Martinez-Treviño, A. El Aroudi, A. Cid-Pastor, and L. Martinez-Salamero, "Nonlinear control for output voltage regulation of a boost converter with a constant power load," *IEEE Trans. Power Electron.*, vol. 34, no. 11, pp. 10381–10385, Nov. 2019.

[25] G. Sulligoi, D. Bosich, G. Giadrossi, L. Zhu, M. Cupelli, and A. Monti, "Multiconverter medium voltage dc power systems on ships: Constant-power loads instability solution using linearization via state feedback control," *IEEE Trans. Smart Grid*, vol. 5, no. 5, pp. 2543–2552, Sep. 2014.

[26] C. N. Onwuchekwa and A. Kwasinski, "Analysis of boundary control for buck converters with instantaneous constant-power loads," *IEEE Trans. Power Electron.*, vol. 25, no. 8, pp. 2018–2032, Aug. 2010.

[27] C. N. Onwuchekwa and A. Kwasinski, "Analysis of boundary control for boost and buck-boost converters in distributed power architectures with constant-power loads," in *Proc. Annu. IEEE Appl. Power Electron. Conf. Expo.*, Mar. 2011, pp. 1816–1823.

[28] L. Benadero, R. Cristiano, D. J. Pagano, and E. Ponce, "Nonlinear analysis of interconnected power converters: A case study," *IEEE J. Emerg. Sel. Topics Circuits Syst.*, vol. 5, no. 3, pp. 326–335, Sep. 2015.

[29] S. Singh, D. Fulwani, and V. Kumar, "Robust sliding-mode control of dc/dc boost converter feeding a constant power load," *IET Power Electron.*, vol. 8, no. 7, pp. 1230–1237, Jul. 2015.

[30] S. Singh and D. Fulwani, "Constant power loads: A solution using sliding mode control," in *Proc. 40th Annu. Conf. IEEE Ind. Electron. Soc.*, Oct. 2014, pp. 1989–1995.

[31] B. A. Unni and P. R. Kumar, "Higher order sliding mode control based duty-ratio controller for the DC/DC buck converter with constant power loads," in *Proc. Int. Conf. Elect., Electron. Optim. Techn.*, Mar. 2016, pp. 656–661.

[32] S. Singh, V. Kumar, and D. Fulwani, "Mitigation of destabilising effect of CPLs in island dc micro-grid using non-linear control," *IET Power Electron.*, vol. 10, no. 3, pp. 387–397, Mar. 2017.

[33] B. A. Martinez-Treviño, A. El Aroudi, E. Vidal-Idiarte, A. Cid-Pastor, and L. Martinez-Salamero, "Sliding-mode control of a boost converter under constant power loading conditions," *IET Power Electron.*, vol. 12, no. 3, pp. 521–529, Mar. 2019.

[34] W. He, R. Ortega, J. Machado, and S. Li, "An adaptive passivity-based controller of a buck-boost converter with a constant power load," *Asian J. Control*, vol. 21, no. 1, pp. 581–595, Mar. 2019.

[35] W. He, C. A. Soriano-Rangel, R. Ortega, A. Astolfi, F. Mancilla-David, and S. Li, "Energy shaping control for buck–boost converters with unknown constant power load," *Control Eng. Pract.*, vol. 74, pp. 33–43, May 2018.

[36] R. D. Middlebrook and S. Cuk, "A general unified approach to modelling switching-converter power stages," in *Proc. IEEE Power Electron. Specialists Conf.*, Jun. 1976, pp. 18–34.
[37] P. A. Ioannou and J. Sun, *Robust Adaptive Control*, vol. 1. Upper Saddle River, NJ, USA: Prentice-Hall, 1996.
[38] C. Y. Chan, S. H. Chincholkar, and W. Jiang, "Adaptive current-mode control of a high step-up DC-DC converter," *IEEE Trans. Power Electron.*, vol. 32, no. 9, pp. 7297–7305, Sep. 2017.
[39] L. Martínez-Salamero, G. García, M. Orellana, C. Lahore, and B. Estibals, "Start-Up control and voltage regulation in a boost converter under sliding-Mode operation," *IEEE Trans. Ind. Electron.*, vol. 60, no. 10, pp. 4637–4649, Oct. 2013.

Blanca Areli Martínez-Treviño received the mechatronics engineering degree from Universidad Autónoma de Puebla, Puebla, Mexico, in 2014, and the Ph.D. degree from Universitat Rovira i Virgili, Tarragona, Spain, in 2019.

She is currently a Research Assistant with the Department of Electronics, Electrical Engineering and Automatic Control, Universitat Rovira i Virgili, where her research interests are in the field of control of power electronics converters.

Abdelali El Aroudi (Senior Member, IEEE) received the graduate degree in physical science from Faculté des Sciences, Université Abdelmalek Essaadi, Tetouan, Morocco, in 1995, and the Ph.D. (hons.) degree in applied physical science from Universitat Politècnica de Catalunya, Barcelona, Spain, in 2000.

From 1999 to 2001, he was a Visiting Professor with the Department of Electronics, Electrical Engineering and Automatic Control, Technical School of Engineering, Universitat Rovira i Virgili (URV), Tarragona, Spain, where he became an Associate Professor in 2001 and a full-time tenure Associate Professor in 2005. His research interests include the field of structure and control of power conditioning systems for autonomous systems, power factor correction, renewable energy applications, stability problems, nonlinear phenomena, bifurcations control.

Dr. El Aroudi was a Guest Editor of the IEEE JOURNAL ON EMERGING AND SELECTED TOPICS ON CIRCUITS AND SYSTEMS Special Issue on Design of Energy-Efficient Distributed Power Generation Systems in 2015, Guest Editor of the IEEE TRANSACTIONS ON CIRCUITS AND SYSTEMS II in 2018, Guest Editor of *Energies* in 2018 and 2019, an Associate Editor of *Electronics Letters* from 2017 to 2020, and *IET Circuits, Systems and Devices* in 2018 and 2019. He currently serves as Associate Editor-in-Chief in IEEE OPEN JOURNAL OF CIRCUITS AND SYSTEMS, Associate Editor in *International Journal of Circuit Theory and Applications*, and IET *Power Electronics* and Topic Editor in *Energies*.

Hugo Valderrama-Blavi (Member, IEEE) is currently an Associate Professor with the Department of Electronic Engineering and Automatic Control, Universitat Rovira i Virgili, Tarragona, Spain, where he is working in the field of power electronics for renewable energy and distributed generation systems, efficient lighting, high voltage gain conversion, and applications for sillicon carbide devices.

Angel Cid-Pastor (Member, IEEE) received graduate degree in Ingeniero en Electrónica Industrial in and in Ingeniero en Automática y Electrónica Industrial in from the Universitat Rovira i Virgili, Tarragona, Spain , 1999 and 2002, respectively, the M.S. degree in design of microelectronics and microsystems circuits from Institut National des Sciences Appliquées, Toulouse, France, in 2003, the Ph.D. degree from Universitat Politècnica de Catalunya, Barcelona, Spain, in 2005, and the Ph.D. degree from Institut National des Sciences Appliquées, Toulouse, France, in 2006.

He is currently an Associated Professor with the Departament d'Enginyeria Electrònica Elèctrica i Automàtica, Escola Tècnica Superior d'Enginyeria, Universitat Rovira i Virgili, Tarragona, Spain. His research interests include the field of power electronics and renewable energy systems.

Enric Vidal-Idiarte (Member, IEEE) received the Licenciado en Informatica and Ph.D. degrees from the Polytechnic University of Catalonia, Barcelona, Spain, in 1993 and 2001, respectively.

He is currently an Associate Professor with the Departament d'Enginyeria Electrònica, Elèctrica i Automàtica, Universitat Rovira i Virgili, Tarragona, Spain, where he is working in the field of digital and robust control of power converters. He is a member of the Research Group on Industrial Electronics and Automatic Control. His main research interests include power conditioning for vehicles, satellites, and renewable energy.

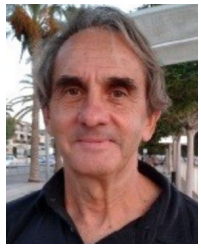

Luis Martinez-Salamero (Senior Member, IEEE) received the Ingeniero de Telecomunicación degree and the Ph.D. degree from the Universidad Politécnica de Cataluña, Barcelona, Spain, in 1978 and 1984, respectively.

From 1978 to 1992, he taught circuit theory, analog electronics and power processing with the Escuela Técnica Superior de Ingenieros de Telecomunicación, Barcelona, Spain. From 1992 to 1993, he was a Visiting Professor with the Center for Solid State Power Conditioning and Control, Department of Electrical Engineering, Duke University, Durham, NC, USA. From 2003 to 2004, 2010 to 2011, and March to September 2018, he was a Visiting Scholar with the Laboratory of Architecture and Systems Analysis (LAAS), National Agency for Scientific Research (CNRS), Toulouse, France. Since 1995, he has been a Full Professor with the Department of Electrical Electronic and Automatic Control Engineering, School of Electrical and Computer Engineering, Rovira i Virgili University, Tarragona, Spain, where he managed the Research Group in Automatic Control and Industrial Electronics (GAEI) from 1998 to 2018. His research interests include structure and control of power conditioning systems, namely, electrical architecture of satellites and electric vehicles, as well as nonlinear control of converters and drives, and power conditioning for renewable energy.